Scripta Materialia 138 (2017) 1–5

Contents lists available at ScienceDirect

Scripta Materialia

journal homepage: www.elsevier.com/locate/scriptamat

Regular Article

Martensite size effects on damage in quenching and partitioning steels

M.-M. Wang [a,b], J.-C. Hell [c], C.C. Tasan [a,*]

[a] Department of Materials Science and Engineering, Massachusetts Institute of Technology, 77 Massachusetts Avenue, Cambridge, MA 02139, USA
[b] Max-Planck-Institut für Eisenforschung, Max-Planck-Straße 1, 40237 Düsseldorf, Germany
[c] ArcelorMittal Global R&D Maizières Automotive Products, Voie Romaine, BP 30320, 57283 Maizières-lès-Metz Cedex, France

ARTICLE INFO

Article history:
Received 2 March 2017
Received in revised form 12 May 2017
Accepted 16 May 2017
Available online xxxx

Keywords:
EBSD
DIC
In-situ
Lath
Strain partitioning

ABSTRACT

Quenching and partitioning steels create new opportunities for light-weight automotive component design, however, a deeper understanding of microstructural damage and failure mechanisms is essential to improve these materials. Here we study the strain partitioning and damage behavior of these steels by carrying out in-situ high resolution microstructure and micro-strain mapping experiments. These investigations reveal that the presence of coarse martensite laths leads to early strain localization, especially when they are in the vicinity of untempered martensite islands. Future alloy design and heat treatment design efforts should thus particularly focus on eliminating copresence of coarse martensite laths and untempered martensite.

Driven by the requirements of lower fuel consumption, reduced CO_2 emission and increased crash safety, advanced high strength steels (AHSS) with high ductility and toughness are highly demanded for light-weighting in automotive industry [1–5]. As a member of 3rd generation AHSS, quenching and partitioning (Q&P) steels have attracted attention due to their combination of low cost and improved properties [3,6–8]. These steels are quenched between M_s and M_f and held at partitioning temperature to stabilize retained austenite by partitioning carbon from martensite [9,10]. The presence of a larger number of thermal treatment parameters motivated several research activities on correlating mechanical properties to microstructural parameters (e.g. volume fraction of retained austenite, carbon content, etc.), to identify treatment pathways for optimal properties [6,8,11–13]. On the other hand, plastic instability, strain localization and failure of such complex microstructures depend also on local microstructural heterogeneities in phase grain size, distribution and morphology, since such heterogeneities typically determine where local strain hardening capacity will be consumed first [14,15]. In fact, proper assessment of failure initiation requires simultaneous probing of the consumption of strain hardening capacity and accumulation of microstructural damage in such zones. For the case of Q&P steels, this means that the transformation of metastable austenite, the strain partitioning between different phases, and the resulting damage mechanisms need to be investigated simultaneously [2,16,17]. The analysis of these phenomena requires in-situ tensile tests with electron backscatter diffraction (EBSD) based microstructure mapping [18–20] and digital image correlation (DIC) based microscopic strain mapping [21,22]. But the spatial resolution of the strain mapping technique is also critical: microscopic-DIC (μ-DIC) measurements based on images of etched surface are able to resolve strain partitioning between polygonal ferrite and martensite-austenite constituents [23], but not between nano-islands of retained austenite and lath martensite [24].

We carried out in-situ SEM deformation experiments with a recently developed contrast- and resolution-optimized μ-DIC method which enables a selective pattern/microstructure imaging strategy [25]. This approach provides direct observation of deformation behavior in each phase and unravels the strain partitioning behavior between nanoscale retained austenite and martensite. The studied Q&P steel is Fe-0.3C-2.5Mn-1.5Si-0.8Cr (wt%). It is a non-commercial grade received in the cold-rolled state from ArcelorMittal R&D Center in France. The heat treatments were carried out in a Bähr dilatometer under vacuum. Samples were austenitized at 1080 °C for 180 s, quenched to 220 °C at 20 °C/s, partitioned at 400 °C for 500 s and eventually quenched to room temperature at 60 °C/s. Samples at this state are referred to as Q&P220 in the following. To characterize microstructure, SEM-based SE imaging, HR-EBSD and XRD measurements were carried out. Samples were prepared following standard metallography methods and finished by polishing with oxide polishing suspension for ~20 min, which ensures removal of surface deformation layer. HR-EBSD measurements were carried out using JEOL JSM-6500F (voltage: 15 KV; working distance: 16 mm; step size: 30 nm). The tensile tests were conducted using Zeiss-FIB SEM with a home-built tensile stage. Firstly, several areas on the polished surface were measured by HR-EBSD. To enable high spatial resolution strain mapping, finely dispersed monolayer of silica particles (diameter ~30–60 nm) was applied on sample surface [25]. For

* Corresponding author.
E-mail address: tasan@mit.edu (C.C. Tasan).

http://dx.doi.org/10.1016/j.scriptamat.2017.05.021
1359-6462/

microstructure-independent pattern imaging of silica particles, HR in-lens SE images were obtained during deformation using an in-lens SE detector (voltage: 1.5 KV; aperture: 30 μm) [25]. Afterwards, these in-lens images were analyzed by Aramis software for calculating strain [26].

The microstructure of Q&P220 consists of tempered martensite matrix, retained austenite (~13.9% by EBSD, 17.9% by XRD) and small amounts of untempered martensite (~2.1% by EBSD) (Fig. 1a). The untempered martensite can be distinguished from tempered martensite matrix due to its lower EBSD image quality [20,27]. Q&P220 exhibits yield stress of 1200 MPa, ultimate tensile stress of 1500 MPa, uniform elongation of 13.4% and total elongation of 21.5%, as shown by an inset in Fig. 1a, but our main focus is on its microstructural response. Fig. 1b shows kernel average misorientation (KAM) map of martensite (i.e. retained austenite is black). KAM is the average misorientation of a given EBSD measurement point with respect to its neighbors. Here 2nd neighbor is considered and misorientations higher than 5° are excluded to eliminate influence of adjacent boundaries. As shown by KAM map, there are several wide regions of lower KAM values embedded in a matrix of higher KAM values. These wide areas of lower KAM correspond to "coarse laths" of martensite, and they have lower hardness and defect density (e.g. ~10% lower dislocation density and ~8% lower hardness in a Fe-0.13C-5.1Ni (wt%) martensitic steel [28]) compared to the matrix of fine martensite laths. This effect is due to a stronger auto-tempering effect, as was studied in detail elsewhere [28]. Based on image analysis of this Q&P steel, the coarse laths have roughly a rectangular prism geometry with two cross sectional dimensions of approximately 2.95 ± 1.01 μm (which is typically at least 3 times wider than the fine laths that constitute the matrix), and the longer dimension that is typically ~3 times this value. A coarse lath region and the austenite distribution therein are shown at higher magnification in Fig. 1c_1 and c_2, respectively; and matrix region with finer laths are shown in Fig. 1d_1 and d_2.

To unravel the influence of microstructure heterogeneity on deformation and damage behaviors, we specifically focus on the presence of these different lath martensite morphologies and characterize two representative areas with and without coarse martensite laths (Fig. 1c_1, d_1) with in-situ deformation experiments. The strain distributions and damage evolutions are shown in Fig. 2. For each area, DIC strain maps with EBSD determined overlay of high angle martensite boundaries (misorientations >15°) (black lines) and austenite/martensite phase boundaries (red lines) are presented.

Upon straining the sample to 1.1% deformation, for the area 1 with the coarse lath, a strain localization band is observed right away along the high angle boundary of coarse martensite lath. The local strain at the band (marked by white solid dots) reaches ~11% already at this low level of deformation (Fig. 2a_2). With increasing global strain to 3.6%, and then to 7.9%, plasticity in this area is mainly localized at these previously formed bands as well as few other points. Maximum local strain in the bands increases to ~25%, then to ~51% (Fig. 2a_3, a_4). In contrast to these bands elongated along the longitudinal direction of coarse martensite laths, the remaining interior of the coarse martensite lath remains at low strain levels (i.e. below ~6%) (Fig. 2a_3, a_4). Similarly, regions with untempered martensite, e.g. located on right side of coarse lath, exhibit low strains (<~5% strain (Fig. 2a_4)). In summary, plastic strain accommodation is highly heterogeneous in the neighborhood of the coarse martensite lath, where highly deformed strain localization bands are sandwiched between zones of low deformation (Fig. 2a_4). Such plastic strain distribution heterogeneities typically lead to initiation of micro-cracking (Fig. 2c_1–c_4), if there is neighboring untempered martensite region (see the yellow arrow). This line of events is confirmed in other zones of similar morphology using post-mortem EBSD measurements.

A different scenario of deformation behavior is observed in area 2, where coarse martensite laths are absent and the microstructure consists of fine martensite laths and retained austenite grains. First of all, following global straining to 1.1%, the average plastic strain level of the whole area 2 (Fig. 2b_2) is clearly lower compared to area 1 (Fig. 2a_2). In fact, based on the local strain levels it seems that the majority of the area is only deformed elastically at this stage. Secondly, plastic deformation is only initiated within retained austenite grains or their close vicinity, demonstrating local strains of up to ~3%. These plastic zones are spots, rather than bands as observed in the case of area 1. With increasing global strain to 3.6%, and then to 7.9%, plastic deformation is

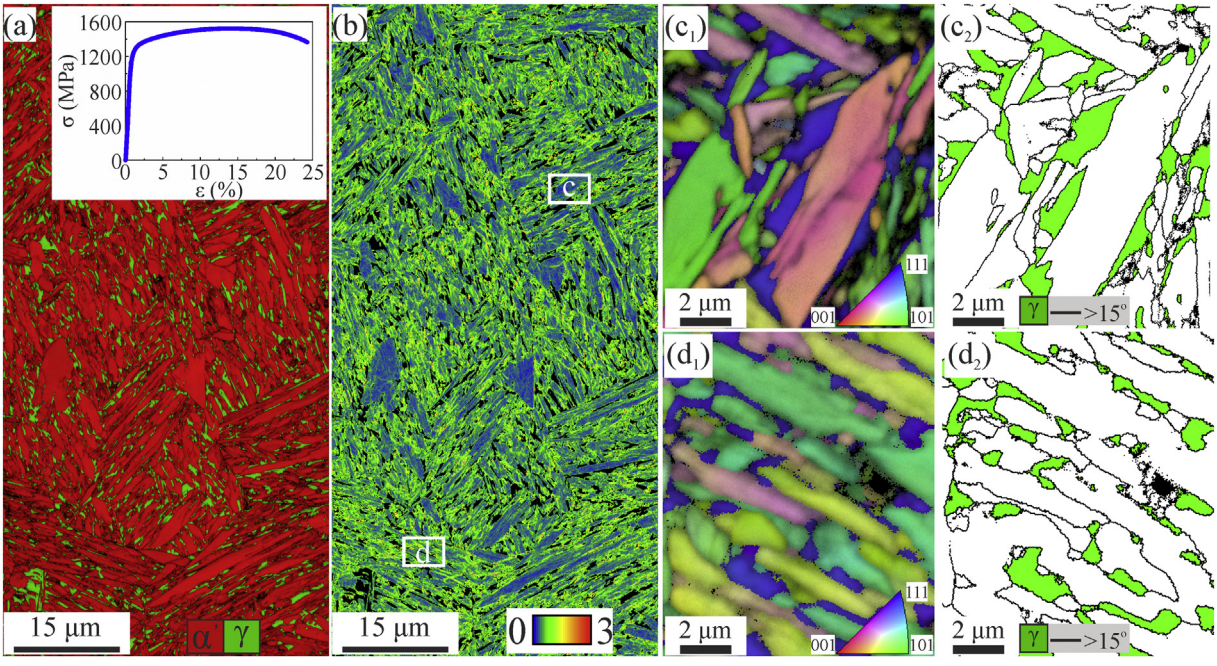

Fig. 1. (a) EBSD phase map with engineering stress-strain curve as inset; and (b) KAM map of martensite. (1) Overlay of image quality with IPF map; (2) austenite phase with high angle boundaries (with misorientations >15°), for (c) coarse lath; and (d) fine lath. Areas shown in (b) only serve to represent that martensite lath type.